Supporting Information

Double Fano Resonances in Hybrid Disk/Rods Artificial Plasmonic Molecules Based on Dipole-Quadrupole coupling

Zhiquan Chen[a,b], Shi Zhang[a], Yiqin Chen[a], Yanjun Liu[c], Ping Li[a], Zhaolong Wang[a], Xupeng Zhu[d], Kaixi Bi[e], and Huigao Duan[a]*

[a] State Key Laboratory of Advanced Design and Manufacturing for Vehicle Body, College of Mechanical and Vehicle Engineering, Hunan University, Changsha 410082, People's Republic of China.

[b] School of Mathematics and Statistics, Hunan University of Technology and Business, Changsha 410205, People's Republic of China.

[c] Department of Electrical and Electronic Engineering, Southern University of Science and Technology, Shenzhen, 518055, People's Republic of China.

[d] School of Physics Science and Technology, Lingnan Normal University, Zhanjiang 524048, People's Republic of China.

[e] Science and Technology on Electronic Test and Measurement Laboratory, School of Instrument and Electronics, North University of China, Taiyuan 030051, People's Republic of China.

* To whom correspondence should be addressed. E-mail: duanhg@hnu.edu.cn (H. D.).

S1: Polarization dependency of the Fano resonance

We further study the transmission characteristics of the artificial plasmonic molecules when the polarization direction is parallel to the gold rod, and all other structural parameters are consistent with those in Figure 2. The transmission spectra of the structures are depicted in Figure S1. The experimental (Figure S1 (a)) and simulated (Figure S1 (c)) transmission spectra of the three structures are roughly the same in shape. Obviously, except a transmission dip, there is no Fano peak appears in the transmission spectra. The transmission dips of the three structures have the same shape and spectral position, which validates that the transmission dip is aroused by the disk. Figure S1 (d) is the surface charge distributions of the structures at four spectral positions (1-4), which are corresponding to the spectral positions of FR1′, FR2′, FR1, and FR2 in Figure 2 (λ_1=1530 nm, λ_2=1730 nm, λ_3=1520 nm, λ_4=1760 nm), respectively. The surface charge distributions at four spectral positions clearly show that a dipole resonance is aroused in the disk, and a broad superradiant mode is formed. However, there are also dipole resonances formed in the two metal rods. In spectral positions 2 and 4, the positive and negative charges form a single dipole at

both ends of the rod. In spectral positions 1 and 3, a pair of dipoles arranged in the same direction on the rod due to the Coulomb attraction of the charges in the disk, leading to a large net dipole moment. There is no destructive interference between the dipole resonance modes in the metal rod and the disk. Therefore, when the polarization direction of the light source is parallel to the metal rods, Fano resonance will not appears in these structures.

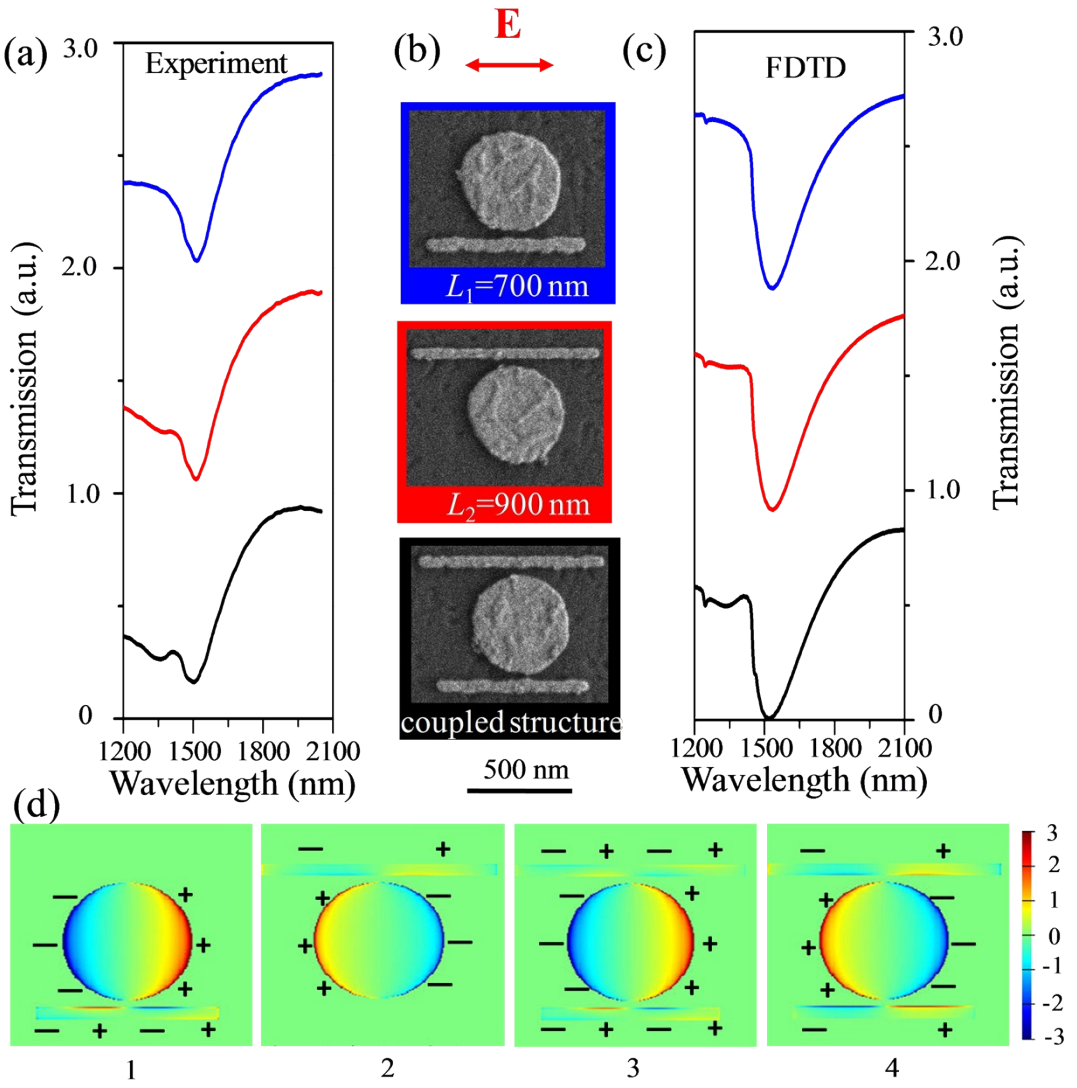

Figure S1. Transmission characteristics of the asymmetric artificial molecule and decomposed structures. (a) Measured transmittance spectra (c) FDTD simulated transmittance spectra. (b) SEM images of the corresponding samples, and the red arrow represents the polarization direction of the electric field. The dimension of the scale bar at the bottom is 500 nm. (d) The surface charge distributions of the structures at 4 spectral positions (λ_1=1530 nm, λ_2=1730 nm, λ_3=1520 nm, λ_4=1760 nm).

S2: The surface charge distributions of the disk

The resonance mode of the disk is further elaborated when the polarization direction of the light source is perpendicular to the rods. As a single disk, the surface charge distributions at four spectral positions (1-4) (which also correspond to the spectral positions of FR1′, FR2′, FR1, and FR2 in Figure 2, respectively.) are shown

in Figure S2. At these four spectral positions, the positive and negative charges in the disk are symmetrically distributed at both ends of the disk, forming a dipole resonance bright mode. Therefore, at the spectral positions FR2′ and FR2 in Figure 2 (d), a partial positive charge distributes at the corresponding coupling position of the disk because of the Coulomb force of the negative charge in the center of the rod 2, and the disk is still dominated by the dipole resonance mode.

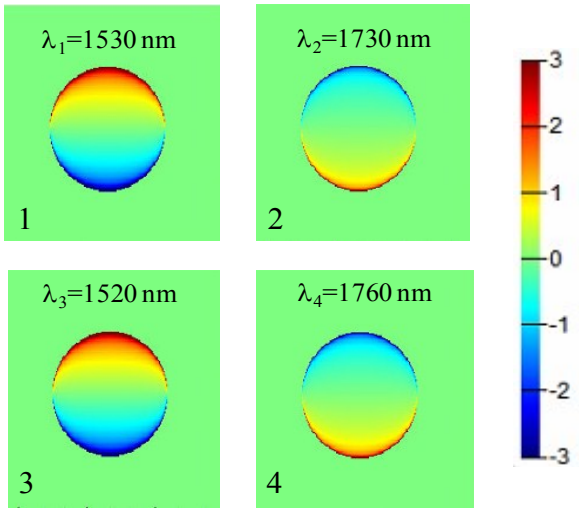

Figure S2. The surface charge distributions of the disk at four spectral positions 1-4 (λ_1=1530 nm, λ_2=1730 nm, λ_3=1520 nm, λ_4=1760 nm).

S3: The model of multimode coupled radiating oscillator theory (MCROT)

In ROT system,[1] there are two resonance modes, a bright mode and a dark mode. The bright mode excited directly by external force $f(t)$ (incident light), and the dark mode excited by the bright mode. In our system, there are three resonance modes, a bright mode of the disk is excited by the incident light, and two dark modes of the two rods are excited by the bright mode. The coupled system can be described as a set of harmonic oscillators[2]:

$$\omega_0^{-2}\frac{d^2}{dt^2}a_0(t)+\gamma_0\omega_0^{-1}\frac{d}{dt}a_0(t)+a_0(t)=f(t)-\kappa_{01}a_1(t)-\kappa_{02}a_2(t), \quad (1)$$

$$\omega_1^{-2}\frac{d^2}{dt^2}a_1(t)+\gamma_1\omega_1^{-1}\frac{d}{dt}a_1(t)+a_1(t)=-\kappa_{01}a_0(t), \quad (2)$$

$$\omega_2^{-2}\frac{d^2}{dt^2}a_2(t)+\gamma_2\omega_2^{-1}\frac{d}{dt}a_2(t)+a_2(t)=-\kappa_{02}a_0(t). \quad (3)$$

The bright mode with resonance frequency ω_0 and damping factor γ_0 is described by the excitation a_0 (t) and driven by the external force $f(t)$. The dark modes with resonance frequency ω_n (n=1, 2,) and damping factor γ_n (i=1, 2) are described by the excitation $a_n(t)$ (i=1, 2). Bright-dark modes are linearly coupled with the coupling strength κ_{0n} (i=1, 2). Equations (1)-(3) can be solved in the frequency domain by assuming a solution of the form $a_N(t)=a_N$

(ω)·exp(-$i\omega t$) (N=0, 1, 2,) and $f(t)=f(\omega)\cdot\exp(-i\omega t)$. As an analogy, the individual oscillators and the excitations can be regard as the electromagnetic elements and the microscopic electric dipole moment, respectively. The effective response of the materials can be described by an electric current sheet with surface conductivity σ_{se}. If each of the meta-atoms generates a dipole moment a_0 with the external field, and there are n_s atoms per unit of surface area, the average polarization current equals

$$\langle j_s(t)\rangle = n_s \frac{d}{dt} a_0(t) = -i\omega n_s a_0(\omega)\,, \tag{4}$$

The driving force f and surface field E_s have the proportional relationship $f(t)$=C $E_s(\omega)$ (C is constant). In addition, for the linear meta-atom, the average dipole moment must be proportional to the electric field at the surface: $n_s a_0(\omega)=\varepsilon_0\chi_{se}(\omega)E_s(\omega)$, where χ_{se} is the surface susceptibility. In the static limit, these yield

$$\varepsilon_0\chi_{se}^{(static)}E_s(0) = n_s a_0(0) = n_s(1-\kappa_{0n}^2)^{-1} f(0) \approx n_s f(0)\,, \tag{5}$$

where κ_{0n}<<1 under EIT conditions in the last approximation. Using Eqs. (4) and (5), the surface conductivity can be deduced from the constitutive equation $<j_s(\omega)>=\sigma_{se}E_s(\omega)$,

$$\sigma_{se} \approx \varepsilon_0\chi_{se}^{(\text{static})}\frac{-i\omega a_0(\omega)}{f(\omega)} = \frac{-i\omega D_1 D_2}{D_0 D_1 D_2 - D_2\kappa_{01}{}^2 - D_1\kappa_{02}{}^2}\,, \tag{6}$$

where $\varepsilon_0\chi_{se}^{(\text{static})}$=1 when in vacuum, and D_N=1-(ω /ω_N)^2-$i\gamma_N$ (ω /ω_N) (N=0, 1, 2,). The transmission can be calculated in the following form

$$T = \left|\frac{2}{2+\xi\sigma_{se}}\right|^2\,, \tag{7}$$

where $\xi=\beta(L)L/\omega\varepsilon_0\varepsilon_i$ is the wave impedance of the external waves, $\beta(L)$ is propagation constant in the coupled cavity, L is the length of the cavity, ε_0 is the permittivity of vacuum. In our simulation, the dielectric is air with the relative permittivity ε_i=1 for simplicity.

S4: Influence of manufacture errors on optical characteristics

All our experimental samples are prepared by electron-beam lithography (EBL), and there are manufacture errors in this process. The roughness of the structure surface and edge is affected by the evaporation rate and vacuum degree in the process of metal thermal evaporation. In view of the manufacture errors in the sample preparation, we make a further study on the influence of the uneven surface and perturbation of structure size on the optical characteristics of the artificial plasmonic molecule. The initial size of the structure is set as: R=250 nm, L_1=700 nm, L_2=900 nm, w=50 nm. In FDTD simulation, the surface roughness of the structure is increased by

adding hemispherical Au particles on the surface of the disk and rod. The radius and number of the Au particles are adjusted and the spectral changes are compared. In addition, by changing the radius of the disk, the length and width of the rod, we compared the transmission spectra of the artificial plasmonic molecule.

Figure S3 shows the transmission characteristics of the artificial plasmonic molecule with rough surface and perturbed structure size. Figure S3 (a) shows the transmission spectra of the structure under different surface roughness. Hemispherical particles with different radii (r=5, 10 nm) and density (or periods, p=50 nm, 25 nm) distributed on the surface of disk and rod. When the particle radius is less than 5 nm, the transmission spectrum hardly changes. With the increase of particle size, the Fano resonance peak shifts slightly. Figure S3 (b) and (d) show the transmission spectra of artificial plasmonic molecule for different length deviation (ΔL= -20~20 nm) and width deviation (Δw= -10~10 nm) of two rods (two rods have the same ΔL and Δw). Figure S3 (c) shows the transmission spectra of artificial plasmonic molecule for different radius deviation (ΔR=-20~20 nm). Through simulation, it is found that when the manufacture error is controlled at about 10 nm, the transmission line shape and the Fano peaks position of the artificial plasmonic molecule are almost unchanged.

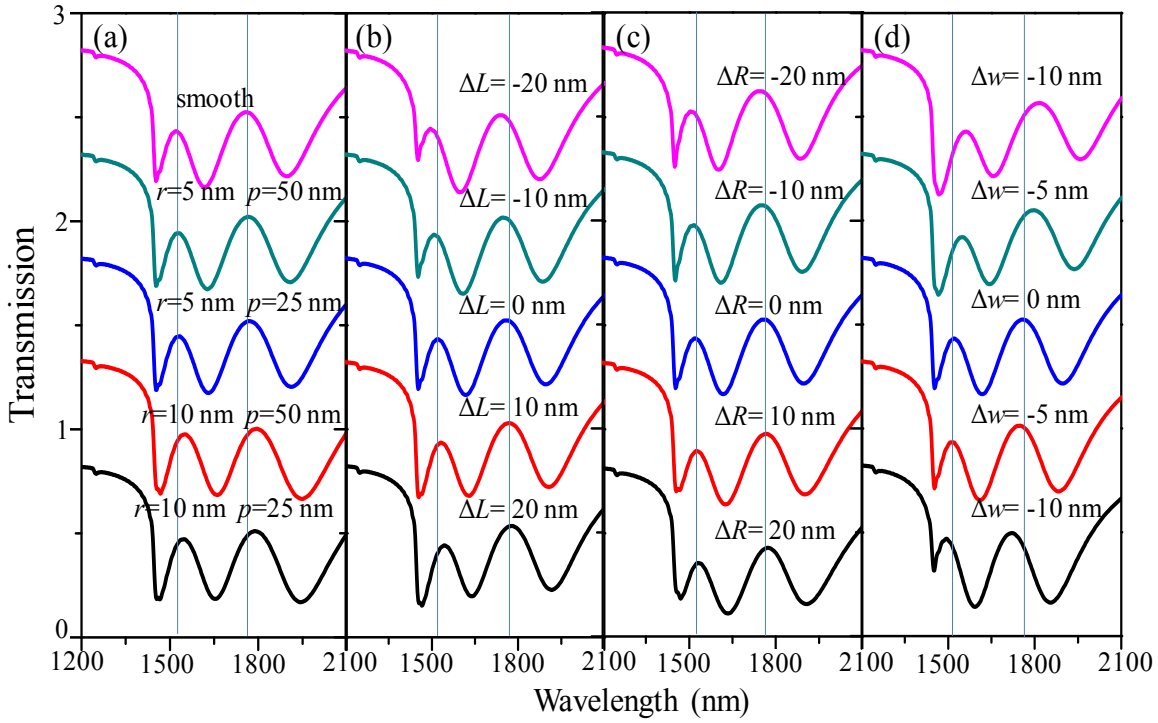

Figure S3 The transmission characteristics of the structure with rough surface and perturbed structure size. (a) Transmission spectra for different surface roughness. (b) Transmission spectra for length deviation (ΔL). (c) Transmission spectra for different radius deviation (ΔR). (d) Transmission spectra for different width deviation (Δw).

References

[1] P. Tassin, L. Zhang, R. Zhao, A. Jain, T. Koschny and C. M. Soukoulis, *Phys. Rev. Lett.*

2012, *109*, 187401.
[2] Z. Chen, H. Li, S. Zhan, B. Li, Z. He, H. Xu, M. Zheng, *Sci. Rep.* **2016**, *6*, 24446.